

# Validation of Opto-Thermal Simulation Techniques for AFP Processing of CF/LM-PAEK Tapes using a Pulsed Xenon Flashlamp System

M Edwards<sup>1</sup>, A Page<sup>1</sup>, A Kolbe<sup>2</sup>, G Fourage<sup>3</sup>, D Williams<sup>1, 4</sup>.

<sup>1</sup>Excelitas Noblelight Ltd, 161 & 163 Science Park, Milton Road, Cambridge, CB4 OGQ, UK

Corresponding author: Michael.edwards@heraeus.com

Keywords: Composite Materials: Automated fibre placement (AFP); Finite element analysis (FEA); Thermal analysis; Thermoplastics.

### **Highlights**

- Full optical characterisation of xenon flashlamp heat source for simulation.
- Validated optical ray tracing simulation, through novel use of a thermal camera.
- Efficiency of process determined through irradiance measurements.
- For the first time, quartz lightquide heating effect included in AFP simulation.
- Accuracy of simulation to within 4.5% established through AFP validation trials.

#### **Abstract**

A simulation tool has been developed for the automated fibre placement (AFP) processing of CF/LM-PAEK (Carbon Fibre/ Low-Melt PAEK) tapes using a pulsed xenon flashlamp heating system. This simulation tool is intended to support the manufacture of thermoplastic fuselage panels. The xenon flashlamp source was characterised using spectral irradiance and goniometry to determine the wavelength and angular distribution of the rays passing through the delivery head of the flashlamp system. The energy levels and irradiance were measured using a thermal camera and were compared with the pattern obtained from the simulation, which demonstrated correlation and meant the energy efficiency of the system could be calculated. CF/LM-PAEK tapes were thermally characterised by laser flash analysis (LFA) and differential scanning calorimetry (DSC) methods, to ensure that the thermal diffusivity parameters were accurate and temperature dependent. Secondary IR heating from the system's quartz lightguide was found, characterised by thermal cameras, and simulated by finite element analysis (FEA). Including this additional heat source as a boundary condition in the "master" FE simulation improved the accuracy of the tool. Verification through thermal camera and thermocouple measurements showed that the simulation tool was accurate to within 4.5% for 2-ply AFP lay-up at different power and speed settings for both ambient and heated tooling.

<sup>&</sup>lt;sup>2</sup>Deutsches Zentrum für Luft und Raumfahrt (DLR), Ottenbecker Damm 12, 21684 Stade, Germany

<sup>&</sup>lt;sup>3</sup>ESTIA Compositadour, Parc Technocité, 1 rue Pierre-Georges Latécoère, 64100 Bayonne, France

<sup>&</sup>lt;sup>4</sup>University of Bath, Department of Mechanical Engineering, Claverton Down, Bath, BA2 7AY, UK



#### Introduction

This work concentrates on developing predictive simulation methods used in the automated fibre placement of CF/LM-PAEK thermoplastics for manufacturing fuselage panels using xenon flashlamp technology.

Thermoplastics, such as CF/LM-PAEK, have been identified as a potential material for the light weighting of fuselage panels, resulting in increased fuel efficiency and lower carbon emissions. Predictive simulation of the AFP processing of CF/LM-PAEK thermoplastics has been identified to help the end user more quickly determine optimal processing conditions, saving time and reducing processing trials.

A pulsed xenon flashlamp heating system (humm3®) has been developed for composite manufacturing via the AFP [1] [2] and filament winding [3] processes. This system has been shown to achieve rapid tape heating, approaching the performance of a laser heating system. Descriptions of previous work using xenon flashlamp systems can be found in previous publications [3] [4] [5]. The xenon flashlamp system energy source consists of a water-cooled xenon flashlamp inside a flow tube as shown in figure 1. The water-cooled lamp is housed in a delivery head, which importantly, from an optical perspective, consists of a reflector and quartz light guide that work together to guide light to the targeted heating areas. For AFP, the targets are the CF/LM-PAEK substrate and incoming tow tapes, as close to the nip point as possible. To ensure that as much energy as possible is directed towards the targets, the tip of the light guide has been cut into an optimised shape, as shown in figure 1. The optical energy is delivered in controllable pulses, with the operator being able to vary pulse, voltage, duration, and frequency parameters. Having three variable pulse parameters maximises processing flexibility and optimisation potential for the operator.

The system has a specifically designed pulsed power supply that can deliver xenon flashlamp pulses more than 100 Hz for an averaged power of 6 kW for a 2" system and 14 kW for a 4" system. This results in the rapid surface heating of thermoplastic composite tapes. Pulsed xenon flashlamp systems have relatively minor safety considerations, such as the thermal hazard of the quartz lightguide, which can reach temperatures of more than 700°C as shown later in this work, and the emission of a small amount of UV-B/C radiation in the spectral output. However, these hazards are localised to a region around the system head, and this means the AFP process does not have to be performed in an enclosed safety chamber. The industrial alternative of laser AFP has a high safety burden, with the AFP process typically being performed in an enclosed safety chamber to guard against unpredictable reflection behaviour resulting from high energy, collimated light striking reflective fibres on the composite surface.

To date, building similar simulation tools for AFP with a pulsed xenon flashlamp system is limited to research outlined in [6]. This work covered numerical theory, pulsed operation and used a representative optical simulation that was subsequently compared to some AFP trials and achieved some physical agreement. The work described in this paper experimentally validates the approach in [6], concentrating on characterising the heat sources and CF/LM-PAEK material rather than the thermal simulation. Furthermore, [6] did not consider the impact of radiative heating from the quartz light guide. For the simulation tool to be accurate and useful to the system operator, it needs to be validated first optically and then thermally. Thirdly, the model needs to be applicable to different power levels with system efficiency well-understood. Finally, all major heating contributions need to be determined and accounted for



within the final simulation. This work starts with the development of a validated optical model of the xenon flashlamp, followed by the discovery and characterisation of a secondary heating source from the quartz lightguide itself, to the development of a robust simulation tool that is shown to be accurate for a variety of AFP layup conditions and tooling temperatures.

There are several examples of FEA and optical ray tracing being combined to simulate the AFP process within the literature for laser sources [7] [8] [9] [10] [11] [12] [13], IR lamp sources [13] [14] [15] [16] and hot gas torches [13] [17] [18] [19]. The approach taken in this work is like that of Stokes-Griffin and Compston [7], where they use commercial finite-element (ANSYS Mechanical) and ray tracing (TracePro) software packages to develop the simulation. There are different thermal simulation approaches shown in the literature. Some authors have used Eulerian approaches, where the mesh remains static and tape motion is included through the addition of an advective term to the heat flow equation, and others have used Lagrangian approaches, where the mesh is deformable. Lagrangian FE simulations have typically been used to investigate roller deformation, thermo-elastic tape parameters and, ultimately, contact time [20] [21] [22].

For the case in this work, where tape temperatures are the target application, Eulerian simulations for processing temperatures [6] [7] [23] are most common, but there are some exceptions. Li et al [8] used an algorithm to activate elements within ANSYS to simulate evolution of the AFP process as plies are added to the layup. Baho et al [9] took an interesting hybrid approach where different parts of the Eulerian and Lagrangian methods are combined. These authors used a semi-analytical approach to determine roller modulus from its deformation with respect to force, then performed ray tracing and thermal simulations with the deformed roller. The ray tracing in [9] was performed as a 2D model, which is acceptable for a laser heat source, but is not appropriate for the diffuse xenon flashlamp system. The approach in [9] allowed for the consideration of compaction force within an Eulerian framework, through performing the ray tracing and thermal part of the simulation on the pre-deformed roller shape.

In this paper, the optical validation of light exiting the pulsed xenon flashlamp source and system head is described by means of the ray tracing simulation. TracePro, a Monte Carlo-based ray tracing package was used for this purpose. The optical source model was developed by characterising the optical source using spectral irradiance and goniometric methods, building optical materials and surface models of the constituent parts of the flashlamp system. Transmission curves were used to build optical material models for the grades of quartz and the water used within the system. The light exiting the pulsed xenon flashlamp system was simulated striking a CF/LM-PAEK target with measured reflectivity and absorption parameters. The simulated irradiance profile was experimentally verified using a thermal camera. The electrical-radiative energy conversion efficiency was then calculated to determine the scaling and power levels required within the thermal simulation.

The thermal aspects were solved using transient thermal simulations within the ANSYS FEA package, calculating the expected processing temperature. There were two separate transient thermal simulations used, one 3D simulation to determine radiative quartz surface heating effects and one final 2D simulation of the AFP process. In



the literature, the AFP process is typically simulated as a 2D problem, although there are some 3D examples [24] [25] [26]. The simulation tool estimates the processing temperature for given choices of flashlamp pulse parameters, so the time required for an operator to determine appropriate operating parameters can be reduced by this predictive tool. To achieve this, the simulation's solution time needs to be reasonably short. In this work, a 2D solution was chosen to keep the memory requirements down whilst achieving simulation convergence. Furthermore, the main heat transfer mechanism is through the tape motion as the process time is too short to see any meaningful lateral conduction of heat. Therefore, for flat AFP lay-ups, a 2D simulation is sufficiently accurate to obtain good temperature predictions.

During characterisation of primary heating via flashlamp irradiation, a secondary heating contribution was detected, and this was determined to originate from the quartz light guide itself. It was found that the light guide itself heats up during the pulsed operation of the flashlamp, and this heat transfers onto the CF/LM-PAEK tape surfaces through IR radiation. This lightguide heating effect is due to a small proportion of exiting optical energy being absorbed by the quartz surfaces. A simulation model incorporating this effect was built and provided an additional boundary condition within the AFP simulation. Finally, the simulation tool was compared with the results from AFP trials to ensure that the tool is valid and provides the system operator with an accurate prediction of processing temperature before commencing physical AFP manufacture.

# **Development of the Xenon Flashlamp Source Model**

#### **Spectral Irradiance Measurements**

To determine the energy emission of a representative flashlamp with respect to wavelength via spectral irradiance measurements, an experiment consisting of a xenon flashlamp within a water-filled clear fused quartz (CFQ) flow tube was built. This is representative of the arrangement inside the flashlamp system head. A Bentham DTMC300 double monochromator was used to measure the spectral irradiance with sufficient detail. The light from the source was captured by a detector 1 m away, and the light was transported via an optical cable into the monochromator system. The double-monochromator then determined the light intensity at a specific wavelength. The system measured the intensity of light with respect to wavelength in 1 nm steps between 200 and 1100 nm, and at 5 nm steps between 1100 and 1700 nm. This gave a detailed spectral irradiance plot of the light source. The spectral emission measurement of the flashlamp with flow tube is shown in figure 2 at three values of the Voltage parameter (100 V, 160 V and 200 V). The measurements in figure 2 show expected flashlamp behaviour, with the 200 V measurement used as the basis for the optical source model [27].

#### Absorption of Light Within the Lamp Envelope and Flow Tube

Before detection by the double monochromator, the light passes through two layers of Heraeus HLQ 200 clear fused quartz (CFQ) glass and a layer of water. Since the spectral emission is broadband, it was prudent to check that these layers were not absorbing significant amounts of energy in the UV and IR regions. The attenuation coefficient, k, with respect to wavelength for water is available in the literature [28] and was calculated for HLQ200 quartz from the transmission curves on the manufacturer's website [29]. The plots of k for both water and HLQ200 quartz are



shown in figure 3 (a) and the refractive indices in figure 3 (b). When including the k values in absorption calculations, the energy losses to absorption are small in the 400 to 1000 nm range, where most of the emissions occurs, and as figure 3 (c) shows, the correction to the emissivity of the optical model is very small, if flashlamp voltage parameter is close to 200V. The corrected spectral results in figure 3(c) have been included as a surface source model within the optical simulation [27].

# **Validation of Optical Ray Tracing Simulation**

To determine experimentally the rotational variation in intensity of the flashlamp (required as input to the optical model), goniometric measurements, defined as. angular spectral irradiance measurements, were performed with the double monochromator. The measurements were achieved by placing the lamp on a manual rotational stage and taking measurements were taken at 5° intervals about the axis of rotation of the stage as shown in figure 4 (a). The total spectral intensity was measured at each angle, then normalised and plotted alongside the simulation and analytical model described in this section.

To complement the rotational stage measurements, an optical ray tracing model was created within TracePro. A sketch of the ray tracing model is shown in figure 4 (a). A perfectly absorbing circular exit surface, defined as a detector, was placed 1m away from the centre of the flashlamp in the same position as the pyroelectric detector in the physical measurements. Further identical detectors were created at  $5^{\circ}$  intervals until there was  $180^{\circ}$  coverage about the required rotational axis, as indicated in figure 4 (a). The xenon plasma was simulated as a cylindrical Lambertian emitter with a cylinder diameter of 7.96 mm and cylinder length of 70 mm, which corresponds to an 8 mm bore flashlamp and 70mm arc length respectively. To get sufficient convergence at the detectors 1 m away, the cylindrical emitter model was set to produce  $2 \times 10^7$  rays. [27]

To further understand this behaviour, a 2D analytical model of a Lambertian point source with rays passing through three media, firstly a 0.5 mm thick quartz layer representing the lamp housing, then a 2 mm water layer including absorption properties and finally a 1 mm quartz layer representing the flow tube was assessed. The analytical model includes the wavelength-dependent attenuation coefficients and refractive indices for both quartz and water, representing the lamp housing and flow tube materials, as shown in figure 3 (a-b). The wavelength dependent refractive index of the quartz was calculated using the Sellmaier equation using the coefficients given in the Heraeus quartz catalogue [30].

The results in figure 4 (b) suggest a Lambertian source with the angular intensity concentrated towards the lower angles by diffraction determined by Fresnel's equations [31]. The close agreement of the three sets of data gives a strong indication that the light source is indeed very close to Lambertian and the current modelling assumption of a perfect Lambertian emitter is valid about the rotational axis. For the example shown in figure 4 (b), a wavelength of 850 nm was selected as it is the midpoint of the region of highest spectral intensity shown in figure 3 (c). This analytical model has been expanded to the entire range of flashlamp wavelengths and includes the absorption data shown in figure 3 (a). The excellent agreement between the ray trace and analytical model acts to validate the ray



tracing model and shows that the simulation approach for the flashlamp/flow tube assembly, where the xenon plasma is treated as a Lambertian volume emitter, is valid [27].

### **Energy Exiting the System Head**

As a final calibration step for the optical system model, the total energy emitted at wavelengths between 250 and 1100 nm from the end of the pulsed xenon flashlamp system quartz light guide was measured using an integrating sphere with a static double monochromator detector attached. An integrating sphere consists of a diffuse spherical reflector with an aperture containing the double monochromator detector and an opening for the light guide. As the diffuse reflecting surface reflects close to 100% of the light, it makes it possible to collect almost the entirety of the light emitted from the source at the detector within the wavelength range [27].

Firstly, the minimum pulse repetition rate of the detector was determined to be 10 Hz, with the measurements shown in figure 5 (a). The top wavelength of 1100 nm meant that all emissions above 1100 nm were missing from the final analysis and the missing emissions were determined to be close to 5% of the total at both 160 and 200 V, based on the spectral irradiance measurements shown in figure 2. Based on these calculations, it was possible to estimate the proportion of rays that were measured exiting the system head compared to the original 'flashlamp with flow tube assembly'. This quantity is referred to as the "optical efficiency" for the purpose of this work. The results from the optical efficiency calculations are shown in table 1 and suggest an optical efficiency between 65.6 and 69.5% [27].

In parallel to the integrating sphere measurements, an optical model of the pulsed xenon flashlamp system was created within TracePro as shown in figure 6 (a). The optical model was designed to be as geometrically close to the actual flashlamp system as reasonably possible, but some simplifications around the lamp model and reflector were needed to avoid issues with intersecting geometries within the optical simulation. The lamp model simplification is the same used for the goniometric validation model shown in figure 4 (b)4 and has therefore been shown to be valid. The plasma is assumed to be non-absorbing (optically thin) and have a refractive index of 1. Based on analysis of the optical opacity of Xenon plasmas with respect to wavelength at different current densities in [32], an optically thin plasma is a reasonable assumption. The spectral data used for the Lambertian emitter at the outer surface of the plasma cylindrical volume is the absorption corrected data at 200V in figure 3 (c). The light guide is assumed to be a generic fused silica (quartz) from the TracePro library [33]. Finally, the reflector is simplified as a specular reflective surface using appropriate parameters from [34]. [27]

Since all rays pass through several media of differing refractive indices, the default TracePro setting of ray splitting enabled and a 5% flux threshold was found to be unsuitable. At these values, the reflected light component at the interface of two differing media with reasonably close refractive indices, such as quartz and water, would be removed from the simulation as this component would have a value less than 5% of the original ray. At the end of the solution, the result was a significant artificial loss of 28% of the original energy due to the flux threshold parameter. It was found that reducing the flux threshold value to an acceptable value from the energy loss perspective, whilst enabling ray splitting, was computationally expensive. Furthermore, there were no scattering



properties within the simulation, the number of initial rays was set at 10<sup>6</sup> and the results from reducing the flux threshold were converging towards the result with ray splitting disabled. Ray splitting was therefore disabled, meaning that the diffraction behaviour of an individual ray within the simulation being determined probabilistically [27].

The ray tracing simulation predicts that 97.8% of the original optical rays exit the lamp/flow tube assembly. This is due to limited absorption of UV and IR energy by the water layer and very small losses in the UV region from the quartz layers. The simulation then predicts that 66.64% of the original optical energy exits the light guide into the integrating sphere. Therefore, the ratio of energy leaving the lamp/flow tube assembly to light exiting the full system into the integrating sphere, which is the same as the "optical efficiency" defined earlier, is 68.02% and this value falls in the range of measured results given in table 1. Finally, figure 5 (b) shows that the energy distribution of the light exiting the flashlamp system in the ray trace is broadly like the spectral irradiance and integrating sphere measurements. Agreement is excellent in the visible part of the spectrum where measurement is more reliable. The areas of most significant variation occur below 350 nm where measurement is difficult and between 800 and 1000 nm where there exist at least 12 visible emission lines and measuring the exact magnitude and position of these peaks is very difficult for a pulsed source. Considering the large number of emission lines will cause variability between results, the agreement between optical model and experiment is excellent. Therefore, this optical model is suitable for the optimisation of AFP layup by a pulsed xenon flashlamp in conjunction with a thermal model developed with the methodology described in [6], [27].

# Distribution of Light Exiting the Quartz Light Guide

The spatial distribution of energy exiting the lightquide tip designed for AFP from the simulation was subsequently experimentally validated using infrared thermography via a thermal camera [35]. Figure 6 (a) shows the predicted energy distribution from the optical simulation and figure 6 (b) is an image of the energy output estimated from photosensitive burn paper. The distributions look similar but required further experimental measurement. Measuring the energy distribution or surface irradiance was not straight forward with available equipment, but a method for estimating the irradiance was determined using a thermal camera. A Micro Epsilon TIM640 thermal camera with a refresh rate of 133 Hz was used for the measurements. The high refresh rate was required to ensure that the temperature measurement was as close to the peak as possible. A single pulse from the xenon flashlamp system of 200 V and 2.5 ms duration was directed at the thermoplastic surface whilst the camera was recording. The thermoplastic sample was then left to cool for approximately one minute before another pulse was directed at the sample, with this process repeated until there were several reliable pulse measurements available. Thermal image stills were captured immediately before and after each pulse, where figure 6 (c) captures a post-pulse image. As shown in figure 6 (c), a line was plotted along the centre of the irradiated zone and was used to capture the thermal profile. For each pulse, the post-pulse temperature was subtracted from the pre-pulse temperature from the entire dataset along the line to give temperature increase, ΔT. Results for three pulses were calculated and showed very little variation between pulses. The next part of the validation was to convert the dT data into irradiance, H, using a simplified version of Spicer's short pulse duration equation for surface boundaries (equation (1)) [36]. Since the pulse



duration is short and the experiment is static, both the convective and advective terms can be neglected, meaning the simplified equation is valid. To simplify this equation further, the critical thickness  $d_c$  of the CF/LM-PAEK tape was derived using equation (2). The thermal diffusivity  $\alpha$  is given in equation (3). The specific heat c, thermal conductivity  $\lambda$ , and thermal diffusivity  $\alpha$  values are shown in figure 9 (d) and (e). For this case  $d_c$  was calculated at 49 µm and as it is less than the 185 µm thickness of the CF/LM-PAEK tape, it can be assumed to be thermally thick. Therefore, the approximation shown in equation (4) can be used to calculate the localized irradiance [36]. For reference, the emissivity  $\varepsilon_f$  for CF/LM-PAEK is approximately 0.85 using the method described in Meister et al [37].

$$\Delta T^{f}(t) = \frac{2\varepsilon_{f}bH}{\beta\sqrt{\pi}} \left[ \left( \sqrt{t + \Delta t} - \sqrt{t} \right) + \sum_{n=1}^{\infty} \left\{ \frac{\Delta t e^{\left( \frac{-\tau_{g}}{t} \right)}}{\sqrt{t}} \right\} \left[ 1 + \frac{2\tau_{n}}{t} \left( 1 - \frac{1}{\pi} \right) \right] \right]$$
 (1)

$$d_c = \frac{\sqrt{\pi \alpha \Delta t}}{1.2} \tag{2}$$

$$\alpha = \frac{\lambda}{\rho c} \tag{3}$$

$$H = \frac{\Delta T_{max} dc\rho}{\varepsilon_f \Delta t} \tag{4}$$

The comparison between the simulation and experimental estimate of irradiance is shown in figure 6 (d) and agreement appears to be excellent with energy levels of the two peaks and fringe positions appearing to line up. The original 4 kW ray trace was scaled to the calculated irradiance, and this gave an electrical to optical energy conversion efficiency of approximately 50%. This conversion efficiency value supports the results produced later in the paper and is line with other examples in the literature [38]. The work undertaken validates the energy profile produced by the optical simulation. The key outcome is that the optical simulation gives an excellent representation of the actual optical output of the system.

# Radiative Heating from the Quartz Block

During early AFP trials, evidence was found through thermal camera analysis and thermocouple measurement that there is a secondary mechanism for heating thermoplastic tapes that occurs before the main heating from xenon flashlamp output. As figure 7 shows, the substrate starts heating earlier than predicted when the opto-thermal simulation includes xenon flashlamp emission alone. Furthermore, thermal camera analysis showed some background heating of AFP samples occurred after the xenon lamp had finished pulsing. Since the secondary heating source was energetic enough to have an impact on processing temperatures, it required experimental characterisation and simulation. Experimental characterisation was achieved using a standard quartz block within an industrial 4-inch diameter xenon flashlamp system. To characterise the quartz block during operation, the Xenon flashlamp was set to flash at close to the theoretical full power (pulse parameters of 219 V, 90 Hz and 2.5 ms) and left to flash in free space. A thermal camera was placed 30 cm from the lightguide tip and targeted at the largest chamfered surface. During the AFP process this surface provides heating to the substrate and is therefore the most important to characterise. The emissivity of quartz was estimated at 0.93 [39] and the maximum surface temperature



was measured as a function of system operating time, as plotted in figure 8 (a). The block heating follows a power law curve, as figure 8 (a) demonstrates, allowing the calculation of block temperature as a function of operating time within a transient thermal FE simulation.

# 3D Radiative Heating Thermal Simulation.

A 3D transient thermal simulation was built within ANSYS to further investigate the radiant heating effect and to provide a heat flux boundary condition for the simulation of the AFP process. The heat flux boundary condition outputs from the ray tracing were scaled according to calculations from the pulse parameters. Firstly, all surfaces exposed to air had natural convection boundary conditions applied. As mentioned previously, the emissivity of CF/LM-PAEK tape was measured at 0.85 using the method described in Meister et al [37]. This value was inputted as a surface boundary condition within the radiation simulation alongside that of quartz. A temperature boundary condition was applied on the long-chamfered surface and the power law equation in figure 8 (a) was used to determine the temperature with respect to time.

Some industrial systems have the capability of heating the tooling under the substrate with the aim of increasing both lay-up speed and quality. The AFP system used in the work has the capability to heat the composite substrate up to 220°C and was required within the simulation by the end-user. To include the effect of heated tooling, the substrate was pre-heated within the simulation to the point where the substrate reached thermal equilibrium. The different tooling conditions investigated were ambient and 220°C tool temperatures. The thermal boundary condition on the quartz block was then activated and the simulation was set to run for the equivalent of 30s heating time. The heat flux along the central line of the substrate surface was calculated at different maximum block temperatures/running times. It was found that the heat flux curve can be scaled with respect to temperature, which is useful when importing the radiative heat flux curve into the AFP simulation for analysis. The effect of 220°C tooling was investigated, and these results are shown in figure 8 (b). The 220°C tooling results show a lower level of heat transfer as expected based on the Stefan-Boltzmann law. The substrate surface heat flux results at all tooling temperatures were captured in a scalable table, used to import the results into the AFP simulation as shown in figure 9 (c).

# Transfer of Heating Contributions to a 2D Transient Thermal Simulation of the AFP Process

The master 2D transient thermal model used to determine processing temperature is an Eulerian simulation with tape motion provided via an advective term in the heat flow equation using the methodology described in Danezis et al [6]. The simulation itself has been implemented within ANSYS workbench with the support of scripts to provide tape motion. PLANE55 elements were chosen for the simulation as they are programmable to include advection within the heat flow equation. A schematic of the master AFP simulation is shown in figure 9 (a), with constituent layers labelled. Tape motion around the more complex, curved tow geometry was achieved by discretising the shape into 10° sections and applying local coordinate systems along the edges parallel to the motion. These geometrical modifications were found to be sufficiently accurate to work with the heat flux boundary condition generated by the optical simulation. The resultant simulation had an excellent representation of the system motion. Results from the



optical and radiative simulations were saved as csv files and transferred to the master ANSYS AFP simulation using the external data function. Samples of CF/LM-PAEK tape were sent to external laboratories for characterization by laser flash analysis (LFA) and differential scanning calorimetry (DSC). The specific heat, given in figure 9 (d), was directly measured by DSC. LFA directly measured the through-plane thermal conductivity, given in figure 9 (e), and thermal diffusivity of the material. Using these measurements and the relationship between the quantities given in equation (3), a full thermal model of the thermoplastic composite was built. Figure 9 (a) shows that there are other constituent materials that need to be modelled within the simulation. The thermal parameters used to describe the thermalimide, fiberglass, silicone roller and aluminium tooling are given in table 2. The fiberglass acts as a thermally insulating barrier' reducing the heat conduction into the aluminium tool and thereby improving the efficiency of the AFP process. Previous work has shown that xenon flashlamp AFP works better at higher frequencies of 60 to 90 Hz and pulse durations of several milliseconds. These settings reduce temperature peaks due to the pulsed nature of the energy, and these can thermally degrade the CF/LM-PAEK tapes [6] [40]. Thermal peaks are very impractical to measure via thermocouples or thermal cameras due to the rapid refresh rate and low latency requirements of the measurement devices. As a result, the simulation was employed to assess these effects more closely. To achieve this capability within ANSYS, a spreadsheet was created to scale the ray tracing result according to pulse parameters and energy levels according to pre-determined energy efficiency measurements from the single flash irradiance experiment. The spreadsheet calculates a ray trace scaling factor, as well as pulse timings, which is copied into the heat flux boundary conditions. Finally, tape velocity can be controlled as a parameter within the advective command scripts in the simulation. This process means that the simulation can in theory be used for any chosen pulse parameters and tape speeds.

#### **Predictions of temperatures around the Nip Point**

# Comparison between thermocouple measurements and the Opto-Thermal Simulation

As a validation exercise, two rounds of AFP trials were performed, firstly using a 2-inch diameter xenon flashlamp system housed at ESTIA Compositadour (Bayonne, France) and secondly on a 4-inch xenon flashlamp system housed at the Center for Lightweight Production Technology (ZLP), German Aerospace Center (DLR) (Stade, Germany). Trials were performed on two sites to ensure the simulation tool is applicable for both types of xenon flash systems. Thermocouples were inserted between the top of the thermalimide layer on the tooling and the first ply of the composite substrate, known as the S-P1 position. The P1-P2 thermocouple position is defined as sitting on the first ply as the 2<sup>nd</sup> ply is deposited via the AFP process. The thermocouple positions are marked on figure 9 (a). The key results from the initial trials are shown in figure 7 (a), with evidence of the radiative quartz block heating effect explored in the previous section. Very importantly, the simulation appears to capture the key elements of the process and temperature levels are in good agreement with the S-P1 thermocouple in both trials (figure 7, figure 10 (c) and (d)).

Through the characterisation experiments and radiative simulations, it is possible to investigate the impact of block heating on the results for both ambient and heated tooling. To see the temperature effects more visibly, figure 10 (a)



and (b) were plotted as midpoint data for the P1-P2 thermocouple. All the plots in figure 10 show the impact that the quartz block temperature has on the processing temperature, with the impact being more pronounced when the tooling is at ambient temperature as seen in figure 10 (a). In this example, increasing the block temperature from 300 to 700°C increased the peak processing temperature by up to 45°C. The equivalent increase in temperature seen for 220°C heated tooling, shown in figure 10 (b), was only 13.15°C in comparison.

Figures 11 (c) and (d) contain comparisons between the experimental and simulated results of the S-P1 thermocouple during P1-P2 layup trials for ambient (c) and 220°C heated (d) tooling. The simulated results are based on a 50% electrical to optical efficiency, quoted in Smith [38] and the estimate calculated when validating the optical output of the system. This conversion efficiency appears reasonable for a 4" width xenon flashlamp system operating close to its maximum power limit, as the results in figure 10 (c) and (d) demonstrate. For both the ambient and heated tooling case, the simulation result is very close to experiment for the S-P1 thermocouple meaning the thermal properties measured for the composite and calculated energy levels are accurate.

# **Comparison between Thermal Camera Analysis and Opto-Thermal Simulation**

To provide surface temperature measurement during trials, an Optris PI thermal camera was precisely aimed at the region between the quartz light guide and nip point as shown in figure 11. The camera was set up in high resolution mode (640 x 160 pixels) with a refresh rate of 125 Hz. During analysis, the temperature on the CF/LM-PAEK surface, indicated in figure 11, was measured with respect to time for the entire lay-up run and the e mean maximum values measured within the grey polygon shown in table 3. The mean maximum is defined as the mean peak layup temperature within the defined area during the entire layup run. For ambient tooling, the typical conditions for the mean maximum surface temperatures were 336.2°C. For 220°C heated tooling, the respective thermal condition was 375.8°C. The results for the surface temperatures broadly agree with the simulation results in figure 10 (a) and (b), where the results for the ambient tooling best matching a quartz temperature of approximately 500 °C. As figure 10 (b) demonstrated, the quartz heating effect is small for 220°C heated tooling and was neglected from the respective results. Furthermore, the results that the simulation tool is extremely accurate for two-ply layup even with different initial substrate temperatures.

As a final validation step, temperature line profiles were measured in the accessible heating regions to determine agreement with the simulation. The position of the line profile is shown on figure 11. Unfortunately, the presence of the quartz light guide and roller obscured the view of the heating region meaning it was only possible to obtain a snippet between 21 and 8 mm from the nip point. The distance between pixels was determined by measuring part of the quartz light guide of a known dimension, yielding 6.28 pixels/mm. Measurements from the thermal camera were taken in clusters of five at random times where the layup was performing regularly. The averaged data from the simulation was then aligned with the raw data from the temperature profiles to determine correlation between experiment and simulation, with two examples plotted in figure 12. The simulation data was averaged because even at 125 Hz, the thermal camera is unable to differentiate between pulses and see peaks. Figure 12 (a) has an example from an ambient tool and figure 12 (b) from a 220°C tool, with the correlation between experiment and simulation being within 4.5% on all measurements.



There appears to be a minor underestimation of temperature for the ambient tool and a minor overestimation for the 220°C heated tool, which is around 5°C in both cases and possibly caused by small changes in CF/LM-PAEK emissivity with respect to temperature. For the 220°C heated tooling case, the surface temperature of the CF/LM-PAEK material exceeds its melting point, and this could result in increased values of emissivity.

Based on all the work presented in this paper, the simulation tool provides a good view of the thermal evolution of the AFP process using a xenon flashlamp system as a heat source up to the nip point. This predictive simulation tool can potentially reduce the need for the end user to perform trials to determine thermal conditions and flashlamp parameters.

## **Estimation of Nip Point Temperature**

The target of this body of work was to provide a predictive tool for nip point temperature like [41]. Determining nip point temperature is complicated due to the roller's shadow blocking the view and issues measuring absolute surface temperatures with thermocouples, as well as the complicated heat transfer relationship between substrate and tow as they are bonded together. The thermal contact between substrate and tow is imperfect and difficult to verify; with examples in the literature showing that the degree of intimate contact is far from ideal after bonding and the presence of voids [18]. To investigate this problem with the simulation tool, the evolution of thermal contact resistance as material passes under the roller would need to be determined and this is non-trivial potential follow-up work. Therefore, for the purposes of validating the model experimentally, the nip point temperature is determined 1 mm before the substrate and tow tapes touch. The rightmost column of table 3 contains the nip point temperature predictions for the system parameters used in the experimental trials assuming a 500°C quartz block temperature. As table 3 demonstrates, the simulation tool achieves a maximum deviation of 12.83°C between experiment and simulation, corresponding to 4.44% in percentage terms. This demonstrates that all the characterisation work, from the spectral irradiance and goniometry, measurement of irradiance exiting the system, through to thermal characterisation of the PAEK material using LFA and DSC techniques has provided accurate properties and results that are very close to experiment. In the future, the authors hope to transfer these techniques to other composite manufacturing methods. These methods include filament winding of hydrogen pressure vessels and other composite materials, such as glass-fibre based thermoplastics.

#### **Conclusions**

The work presented in this paper has shown that it is possible to create a highly accurate simulation tool of the AFP lay-up process when using a xenon flashlamp system using finite element and ray tracing simulation techniques. The optical output of the xenon flashlamp has been measured through spectral irradiance and goniometry. The input power was determined, and irradiance was calculated by measuring the increase of temperature through a thermal camera. This validated the energy output and optical energy distribution, meaning the irradiance output from the optical simulation was used as a boundary condition in the transient thermal FE simulation. Correlation between the simulation and experimental characterisations described in this paper are excellent, giving the end-user confidence in using this tool to determine layup parameters and processing temperatures.



#### Acknowledgements

This project has received funding from the Clean Sky 2 Joint Undertaking under the European Union's Horizon 2020 research and innovation programme under grant agreement No 886549.

#### References

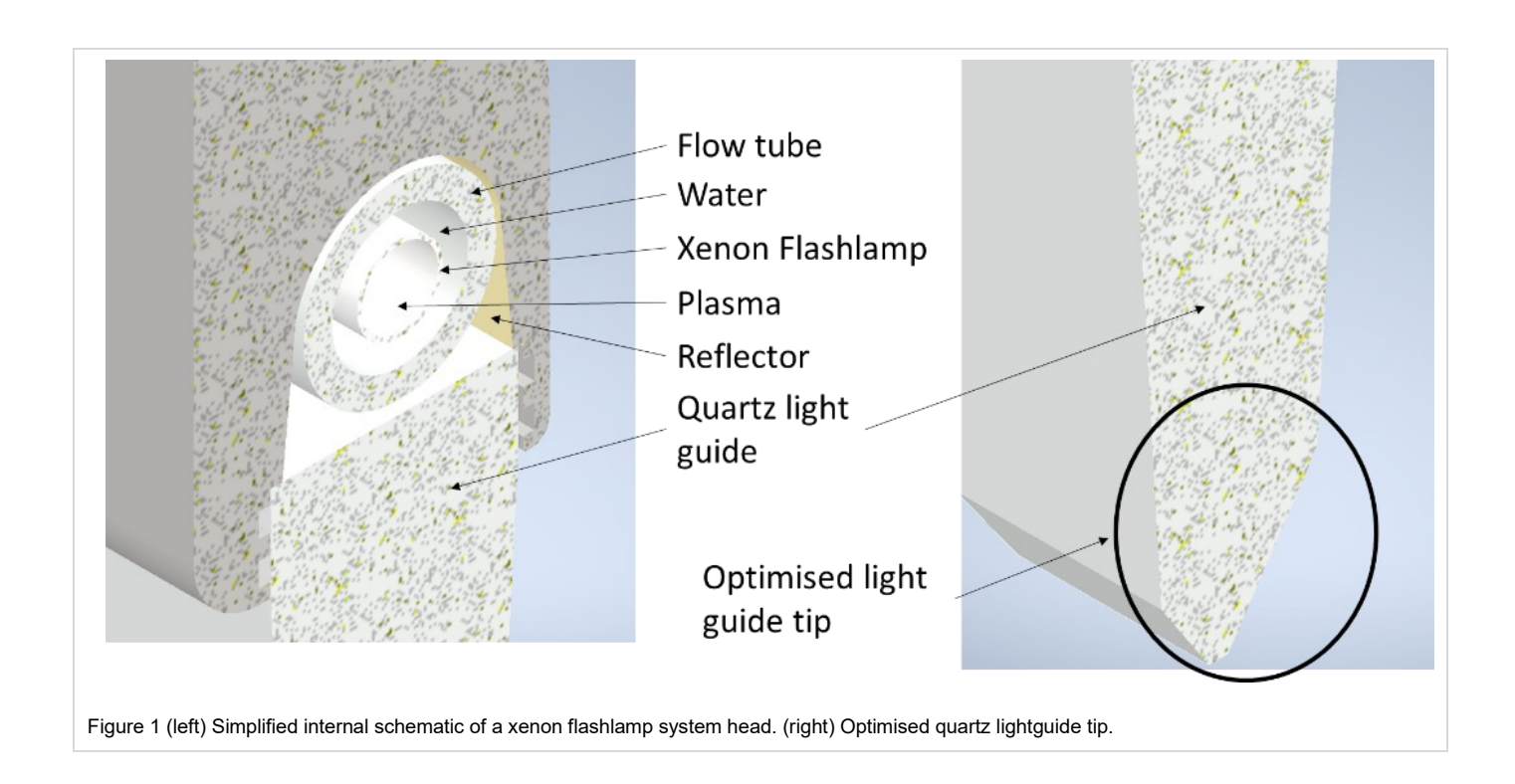
- Lukaszewicz DH-JA, Ward C, Potter KD. The engineering aspects of automated prepreg layup: History, present and future, Composites Part B: Engineering, 43, 3, (2012), p. 997-1009, https://doi.org/10.1016/j.compositesb.2011.12.003.
- [2] Williams D, Brown M. Xenon Flashlamp Heating for Automated Fibre Placement. Third Int. Symp. On Automated Composites Manufacturing, Montreal, Canada, April 20-21 2017
- [3] humm3™ Intelligent heat for Automated Fibre Placement (AFP). < https://www.heraeus.com/en/hng/products\_and\_solutions/arc\_and\_flash\_lamps/humm3/humm3.html>; June 2023
- [4] Monnot P, Williams D, and Di Francesco M. Power Control of a Flashlamp-based Heating Solution for Automated Dry Fibre Placement. In: 18<sup>th</sup> European Conference on Composite Materials. Athens, 2018.
- [5] Brown M, Monnot P, and Williams D. Developments in Xenon flashlamp heating for automated fibre placement. In: Fourth International Symposium on Automated Composites Manufacturing, Montreal, 2019.
- [6] Danezis A, Williams D, Edwards M, and Skordos AA. Heat transfer modelling of flashlamp heating for automated tape placement of thermoplastic composites, Composites Part A: Applied Science and Manufacturing, 145, (2021), 106381.
- [7] Stokes-Griffin CM, and Compston P. A combined optical-thermal model for near-infrared laser heating of thermoplastic composites in an automated tape placement process, Composites Part A: Applied Science and Manufacturing, 75, (2015), p. 104–15.
- [8] Li Z, Yang T, Du Y. Dynamic finite element simulation and transient temperature field analysis in thermoplastic composite tape lay-up process, J. Thermoplast. Compos. Mater. 2015, 28, 558–573.
- [9] Baho O, Ausias G, Grohens Y, et al. Simulation of laser heating distribution for a thermoplastic composite: effects of AFP head parameters. Int J Adv Manuf Technol 110, 2105–2117 (2020). https://doi.org/10.1007/s00170-020-05876-9
- [10] Maurer D, Mitschang P. Laser-powered tape placement process simulation and optimization. Adv. Manuf. Polym. Compos. Sci. 2015, 1, 129–137
- [11] Köhler B, Noeske A, Kindervater T, Wessollek A, Brand T, Biesenbach J. 11-kW direct diode laser system with homogenized 55 \_ 20 mm 2 top-hat intensity distribution. In High-Power Diode Laser Technology and Applications V; International Society for Optics and Photonics: Bellingham,WA, USA, 2007; Volume 6456, p. 64560O.
- [12] Homburg O, Bayer A, Mitra T, Meinschien J, Aschke L. Beam shaping of high-power diode lasers benefits from asymmetrical refractive microlens arrays, In High-Power Diode Laser Technology and Applications VI; International Society for Optics and Photonics: San Jose, CA, USA, 2008; Volume 6876.
- [13] Martin I, Saenz del Castillo D, Fernandez A, Güemes A. Advanced Thermoplastic Composite Manufacturing by In-Situ Consolidation: A Review. Journal of Composites Science. 2020; 4(4):149. https://doi.org/10.3390/jcs4040149
- [14] Lichtinger R, Hörmann P, Stelzl D, Hinterhölzl R. The effects of heat input on adjacent paths during Automated Fibre Placement, Composites Part A: Applied Science and Manufacturing, 68, (2015), p.387-397.
- [15] Hörmann P, Stelzl D, Lichtinger R, Van Nieuwenhove S, Mazón Carro G, Drechsler K. On the numerical prediction of radiative heat transfer for thermoset automated fiber placement, Composites Part A: Applied Science and Manufacturing, 67, (2014), p. 282-288, https://doi.org/10.1016/j.compositesa.2014.08.019.
- [16] Wang H, Wang W, Wang H, Dong H, Ke Y. Thermal management for thermoset automated fiber placement based on infrared heater structure arrangement, Chinese Journal of Aeronautics, 35, 1, (2022), p. 173-183, https://doi.org/10.1016/j.cja.2020.09.017.
- [17] Tierney J, Gillespie Jr JW. Modeling of in situ strength development for the thermoplastic composite tow placement process. Journal of Composite Materials. (2006) ;40(16):1487-
- [18] Tierney J, Gillespie Jr JW. Modeling of heat transfer and void dynamics for the thermoplastic composite tow-placement process. Journal of Composite Materials. 2003 Oct;37(19):1745-68
- [19] Kim HJ, Kim SK, Lee WI, A study on heat transfer during thermoplastic composite tape lay-up process, Experimental Thermal and Fluid Science, 13, 4, (1996), p. 408-418, https://doi.org/10.1016/S0894-1777(96)00095-7.
- [20] Lukaszewicz DH-JA, Potter K. Through-thickness compression response of uncured prepreg during manufacture by automated layup, Proceedings of the Institution of Mechanical Engineers, Part B: Journal of Engineering Manufacture, 226, 2, (2012), p. 193–202. https://doi.org/10.1177/0954405411411817
- [21] Lichtinger R, Lacalle J, Hinterhölzl R, Beier U and Drechsler K, Simulation and experimental validation of gaps and bridging in the automated fiber placement process *Science and Engineering of Composite Materials*, 22, 2, (2015), p. 131-148, https://doi.org/10.1515/secm-2013-0158
- [22] Bakhshi N and Hojjati M. 'Effect of compaction roller on layup quality and defects formation in automated fiber placement', Journal of Reinforced Plastics and Composites, 39(1–2), (2020), p. 3–20, doi: 10.1177/0731684419868845.

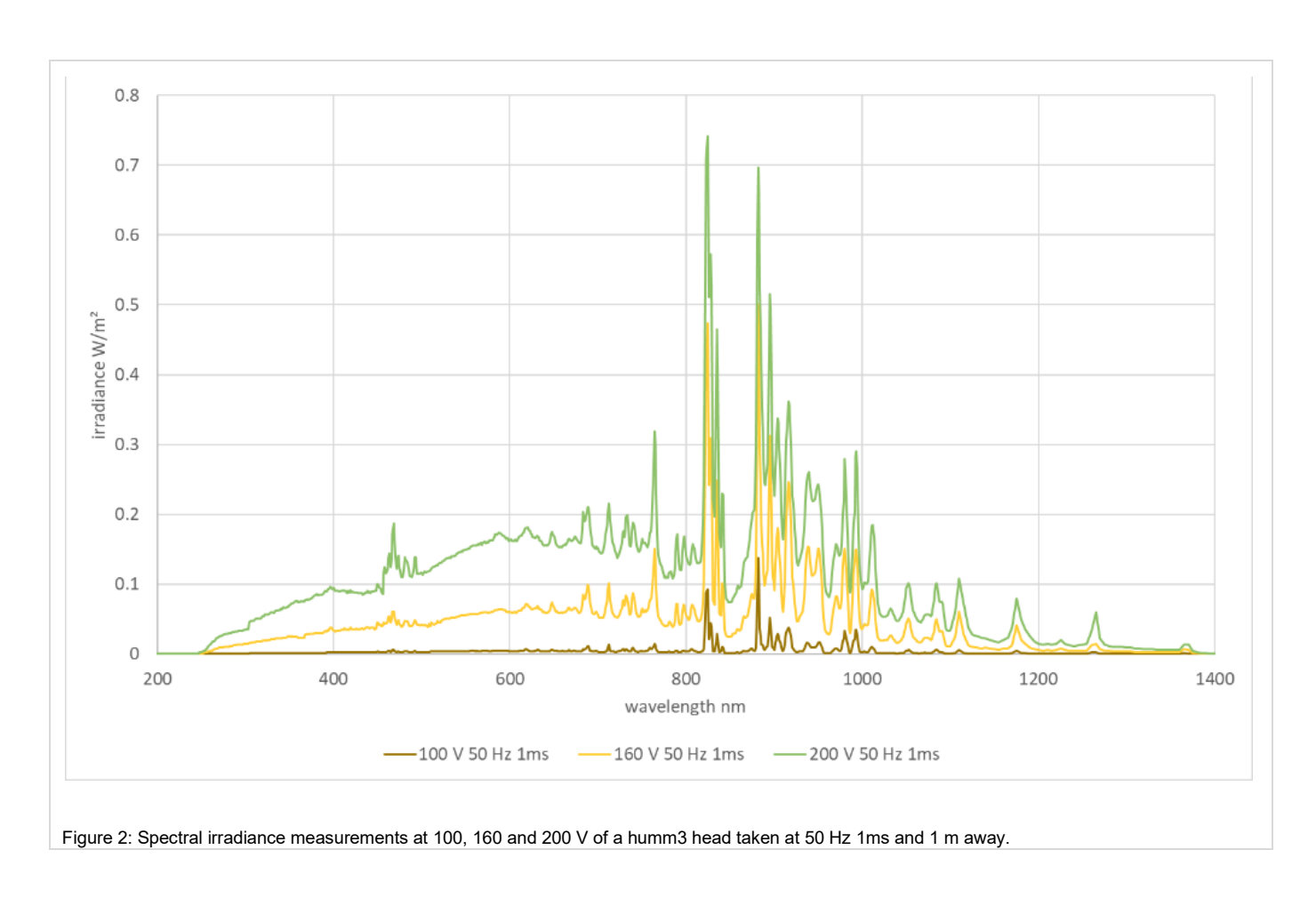




- [23] Stokes-Griffin CM, Compston P, Matuszyk Tl and Cardew-Hall MJ, "Thermal modelling of the laser-assisted thermoplastic tape placement process", Journal of Thermoplastic Composite Materials, 2015, Vol. 28(10) 1445–1462
- [24] Chinesta F, Leygue A, Bognet B, et al. First steps towards an advanced simulation of composites manufacturing by automated tape placement. Int J Mater Form 7, 81–92 (2014). https://doi.org/10.1007/s12289-012-1112-9
- [25] Schledjewski R, Latrille M. Processing of unidirectional fiber reinforced tapes—fundamentals on the way to a process simulation tool (ProSimFRT), Composites Science and Technology, 2003,63 (14), p.2111-2118, https://doi.org/10.1016/S0266-3538(03)00108-8.
- [26] Beyeler EP, and Guceri SI. (May 1, 1988). "Thermal Analysis of Laser-Assisted Thermoplastic-Matrix Composite Tape Consolidation." ASME. J. Heat Transfer. May 1988; 110(2): 424–430. https://doi.org/10.1115/1.3250502
- [27] Edwards M, Page A, Williams D, Danezis A, Schilling M, Jenek T, Optimization of Xenon Flashlamp heating in Thermoplastic Automated Fibre Placement, CAMX The Composites and Advanced Materials Expo Conference Proceedings. Dallas, TX, October 19-21, 2021.
- [28] Hale GM, and Querry MR. Optical Constants of Water in the 200-nm to 200-µm Wavelength Region, Applied Optics, 12 (3), (1973), p.555 563.
- [29] Heraeus Conamic Transmission Calculator for Lamp Applications / Lamp Manufacturing 
  <a href="https://www.heraeus.com/en/hca/fused\_silica\_quartz\_knowledge\_base\_1/t\_calc\_1/transmission\_calc\_lamp/transmission\_calculator\_lm.html">https://www.heraeus.com/en/hca/fused\_silica\_quartz\_knowledge\_base\_1/t\_calc\_1/transmission\_calc\_lamp/transmission\_calculator\_lm.html</a>; May 2021
- [30] Quartz Glass for Optics: Data and Properties, Heraeus Conamic, Accessed from < https://www.heraeus.com/media/media/hca/doc\_hca/products\_and\_solutions\_8/optics/Data\_and\_Properties\_Optics\_fused\_silica\_EN.pdf>; May 2021
- [31] Yu FTS, and Yang X. Introduction to Optical Engineering, 1st Edition, 1997, Cambridge University Press, ISBN: 0-521-57493-5.
- [32] Emmett JL, Schawlow AL, and Weinberg EH. Direct Measurement of Xenon Flashtube Opacity, Journal of Applied Physics 35, 2601-2604 (1964) https://doi.org/10.1063/1.1713807
- [33] TracePro®. <www.lambdares.com/tracepro/>; 2018.
- [34] Rakić AD, Djurisic AB, Elazar JM, and Majewski ML. Optical properties of metallic films for vertical-cavity optoelectronic devices, Applied Optics 1998; 37 (22): 5722-83.
- Usamentiaga R, Venegas P, Guerediaga J, Vega L, Molleda J and Bulnes FG. Infrared Thermography for Temperature Measurement and Non-Destructive Testing, Sensors 2014, 14, 12305-12348; doi:10.3390/s140712305
- [36] Koshti AM. Estimating temperature rise in pulsed thermography using irreversible temperature indicators, Proc. SPIE 4702, Smart Nondestructive Evaluation for Health Monitoring of Structural and Biological Systems, (11 June 2002); https://doi.org/10.1117/12.469878
- [37] Meister S, Kolbe A, Groves RM. Reflectivity and emissivity analysis of thermoplastic CFRP for optimising Xenon heating and thermographic measurements, Composites Part A: Applied Science and Manufacturing, 158, (2022), 106972, https://doi.org/10.1016/j.compositesa.2022.106972.
- [38] Smith B. "Overview of Flashlamps And Arc Lamps," Proc. SPIE 0609, Flashlamp Pumped Laser Technology, (30 June 1986); doi:10.1117/12.966620
- [39] Petrov V and Reznik VY. (1972). Measurement of the emissivity of quartz glass. High Temperatures-High Pressures. V. 4. Pp. 687-693.
- [40] Çelik O, Hosseini SMA, Baran I, Grouve WJB, Akkerman R, Peeters DMJ, et al., The influence of inter-laminar thermal contact resistance on the cooling of material during laser assisted fiber placement, Composites Part A: Applied Science and Manufacturing, 145, (2021), 106367, https://doi.org/10.1016/ji.compositesa.2021.106367.
- [41] Di Francesco M, Veldenz L, Dell'Anno G, and Potter, K. Heater power control for multi-material, variable speed Automated Fibre Placement. Composites Part A: Applied Science and Manufacturing. (2017) DOI: 10.1016/j.compositesa.2017.06.015









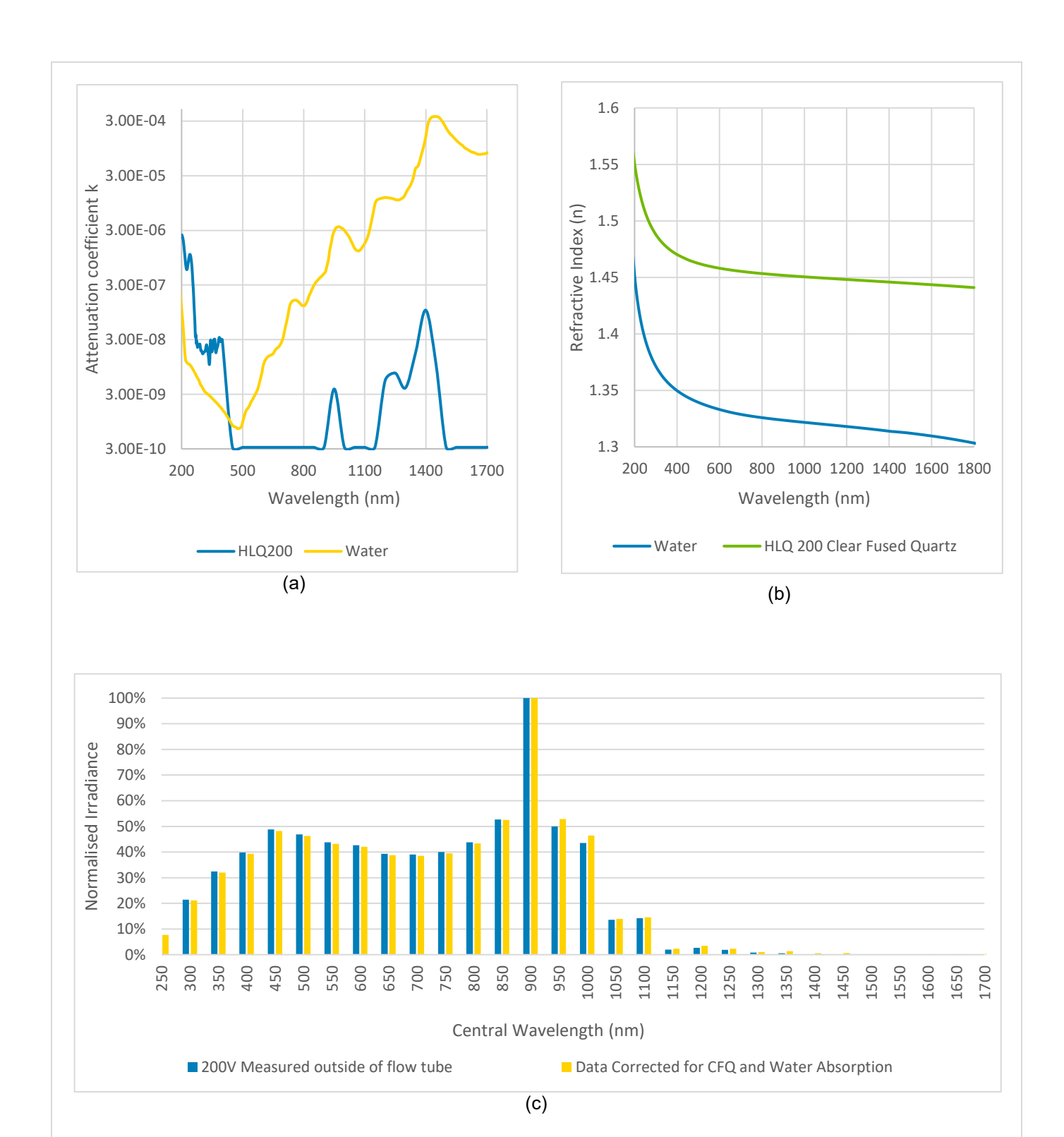


Figure 3: (a) Attenuation coefficient (k) of water and HLQ 200 clear fused quartz (CFQ) used in the manufacturing for the xenon flashlamp and flow tube assembly. (b) Refractive indices of HLQ200 CFQ and water with respect to wavelength. (c) Absorption correction of both quartz and water applied to the xenon flashlamp spectra used in the optical simulations.



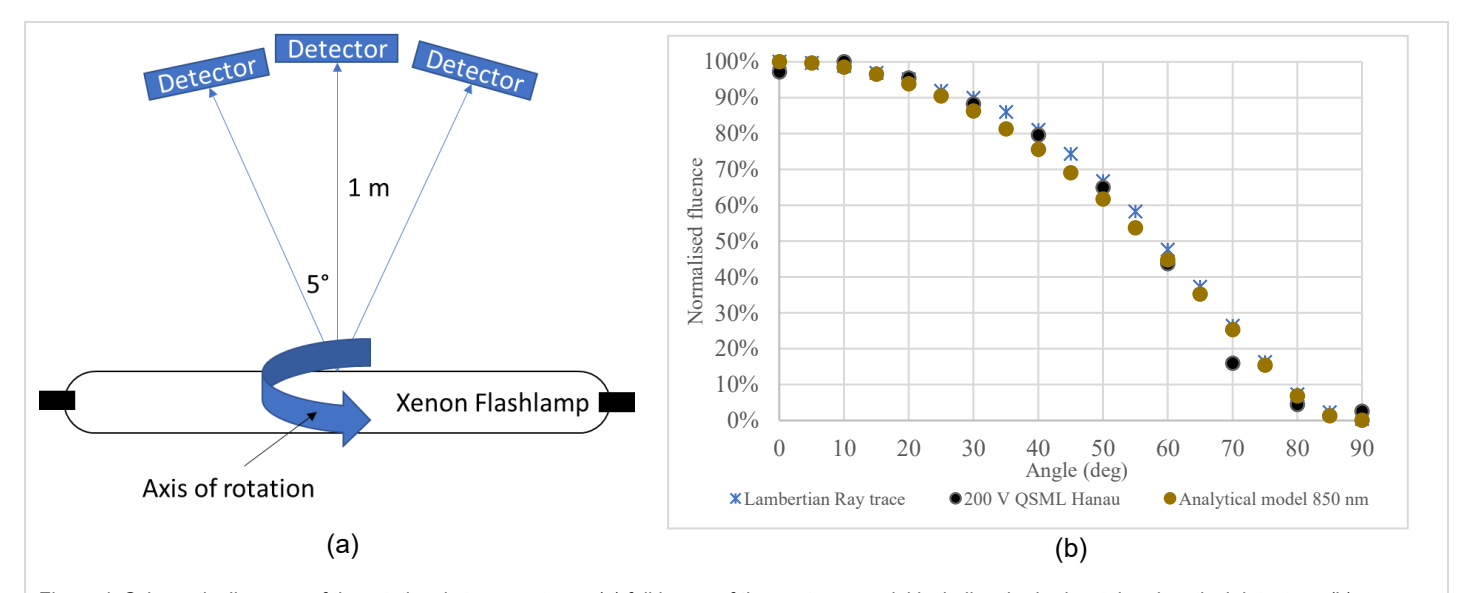


Figure 4: Schematic diagrams of the rotational stage ray trace. (a) full image of the ray trace model including the horizontal and vertical detectors. (b) Normalised comparison between the goniometric measurement of the 'lamp with flow tube' setup measured at 200V 50Hz 1ms with a ray trace of a Lambertian volume emitter and a 2D analytical model of a Lambertian point source with rays passing through the flashlamp/flow tube assembly.

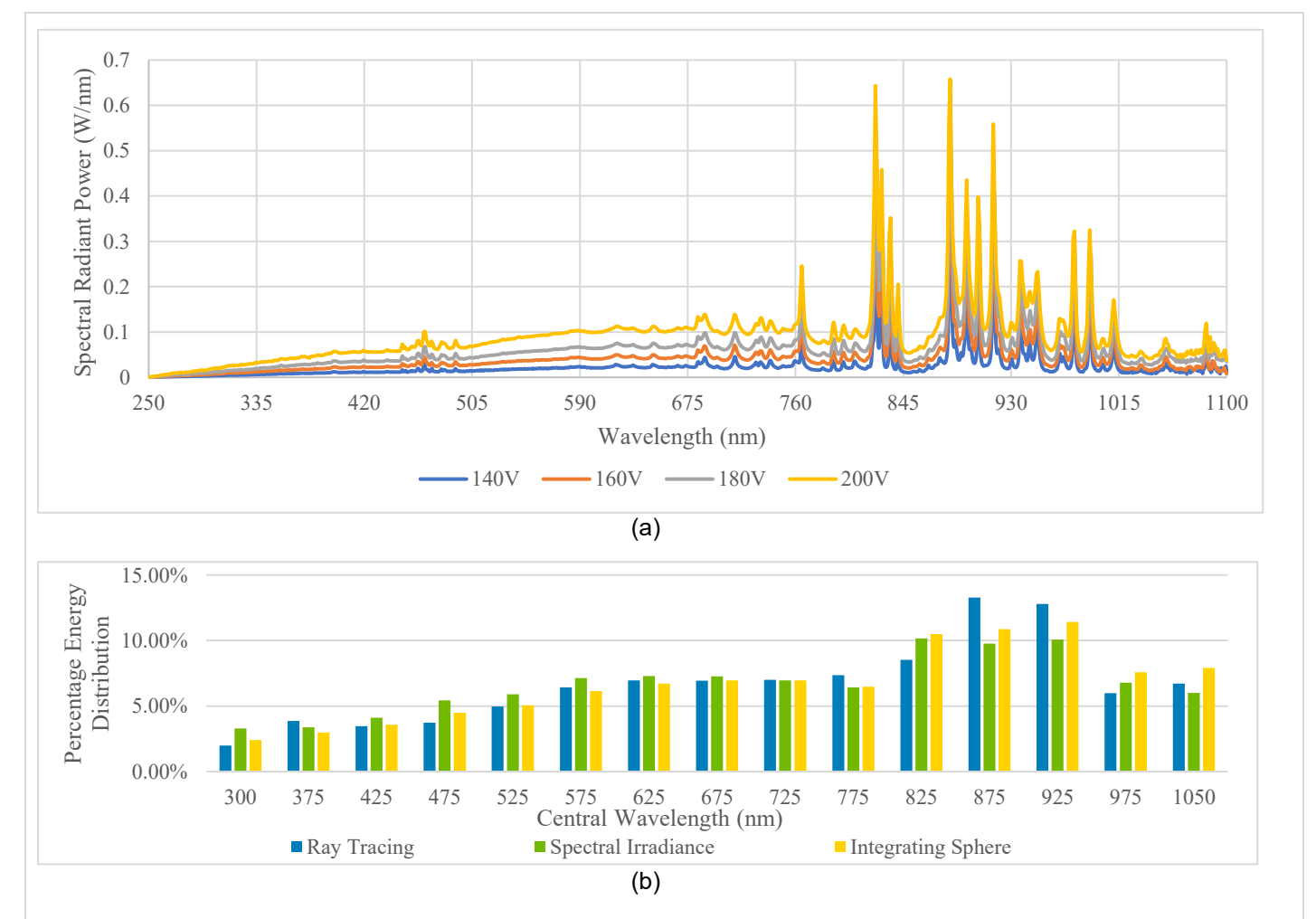
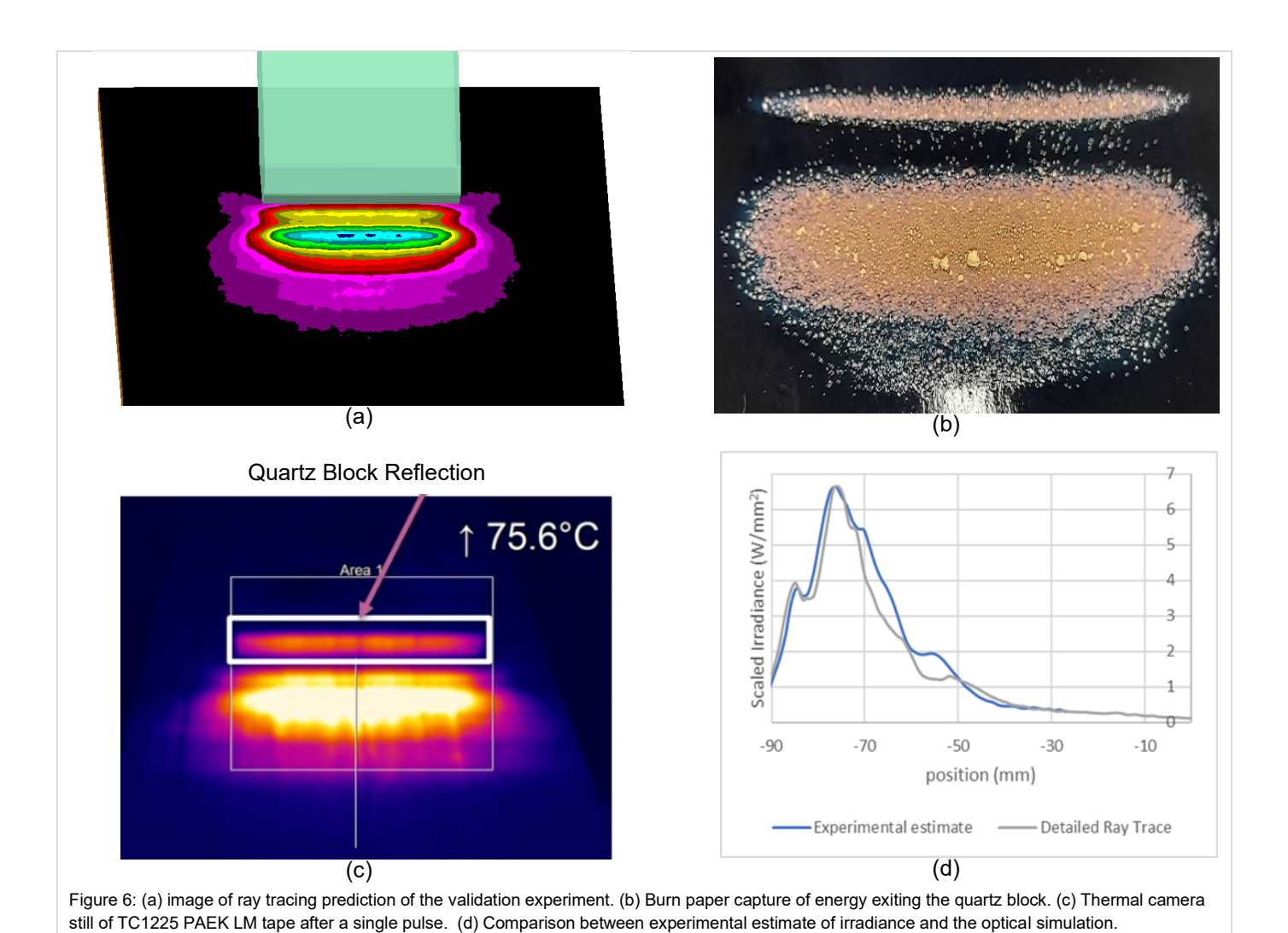
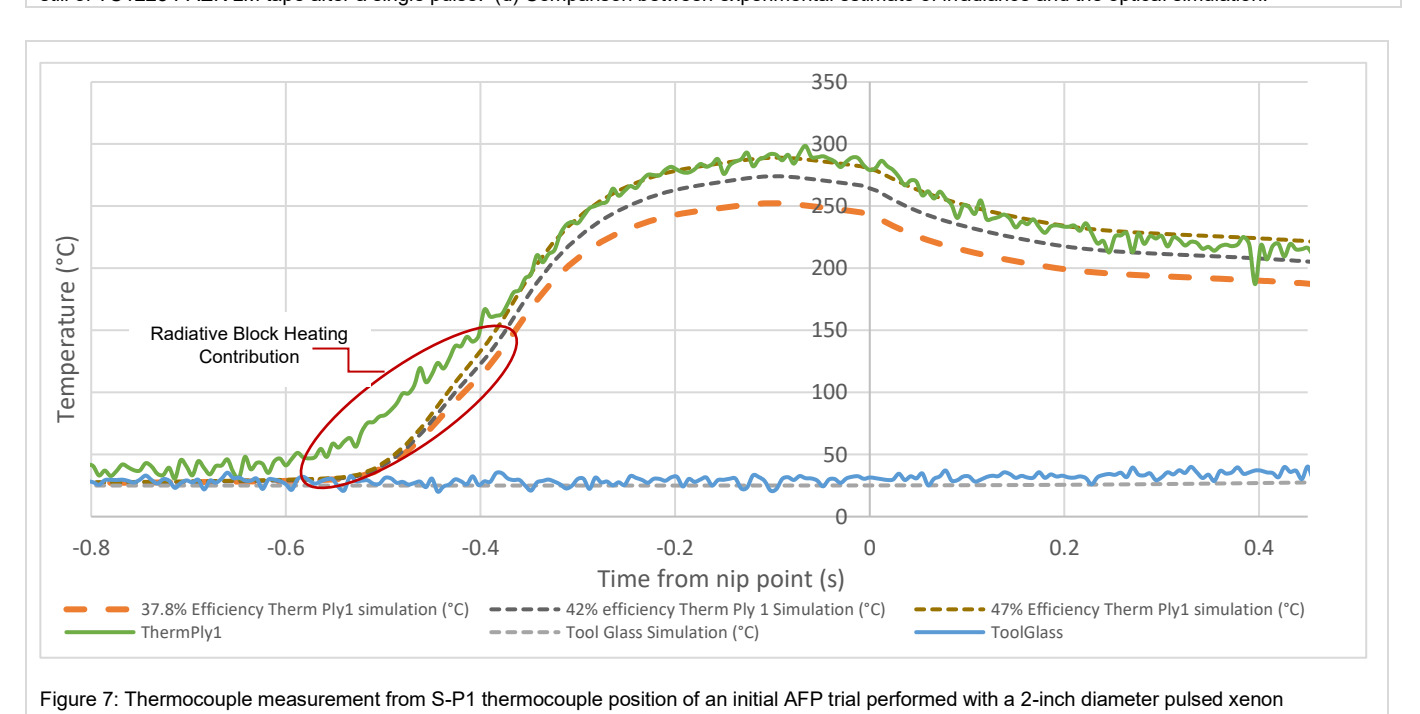


Figure 5. (a) Spectral radiant power measurements taken by the integrating sphere at 10 Hz 1ms between 140 and 200 V set voltage. (b) Percentage energy distribution of light exiting the flashlamp system at 200V from the ray trace, spectral irradiance measurement in figure 2 (a) and integrating sphere in figure 5.



flashlamp (humm3®) system.







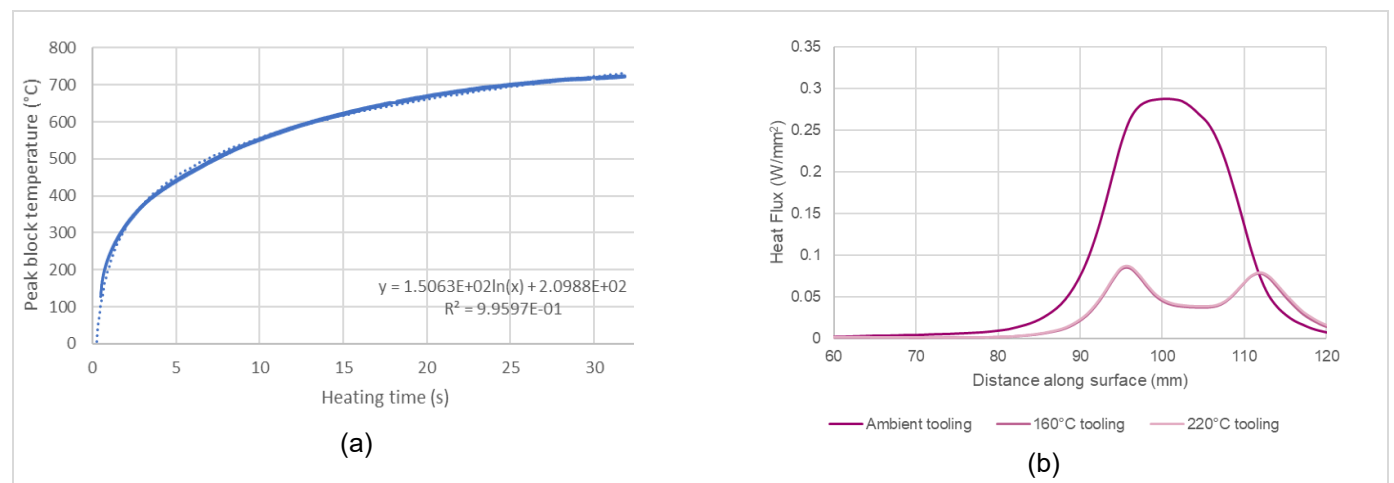
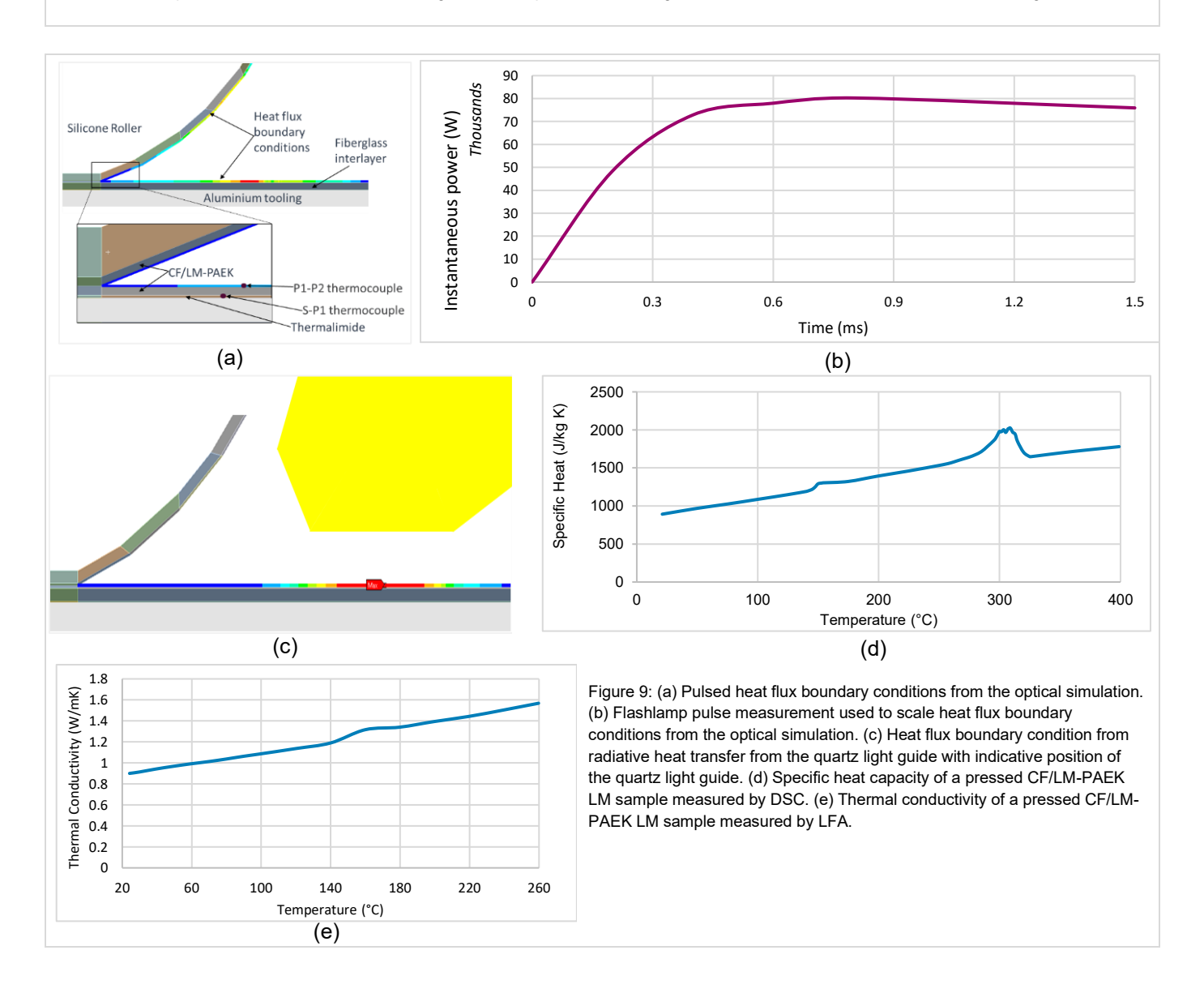


Figure 8: (a) Plot of maximum block temperature of a typical quartz light guide with respect to operating time. (b) Comparison between heat flux at 700°C block temperature for different substrate tooling surface temperatures, showing the difference between ambient and heated tooling.





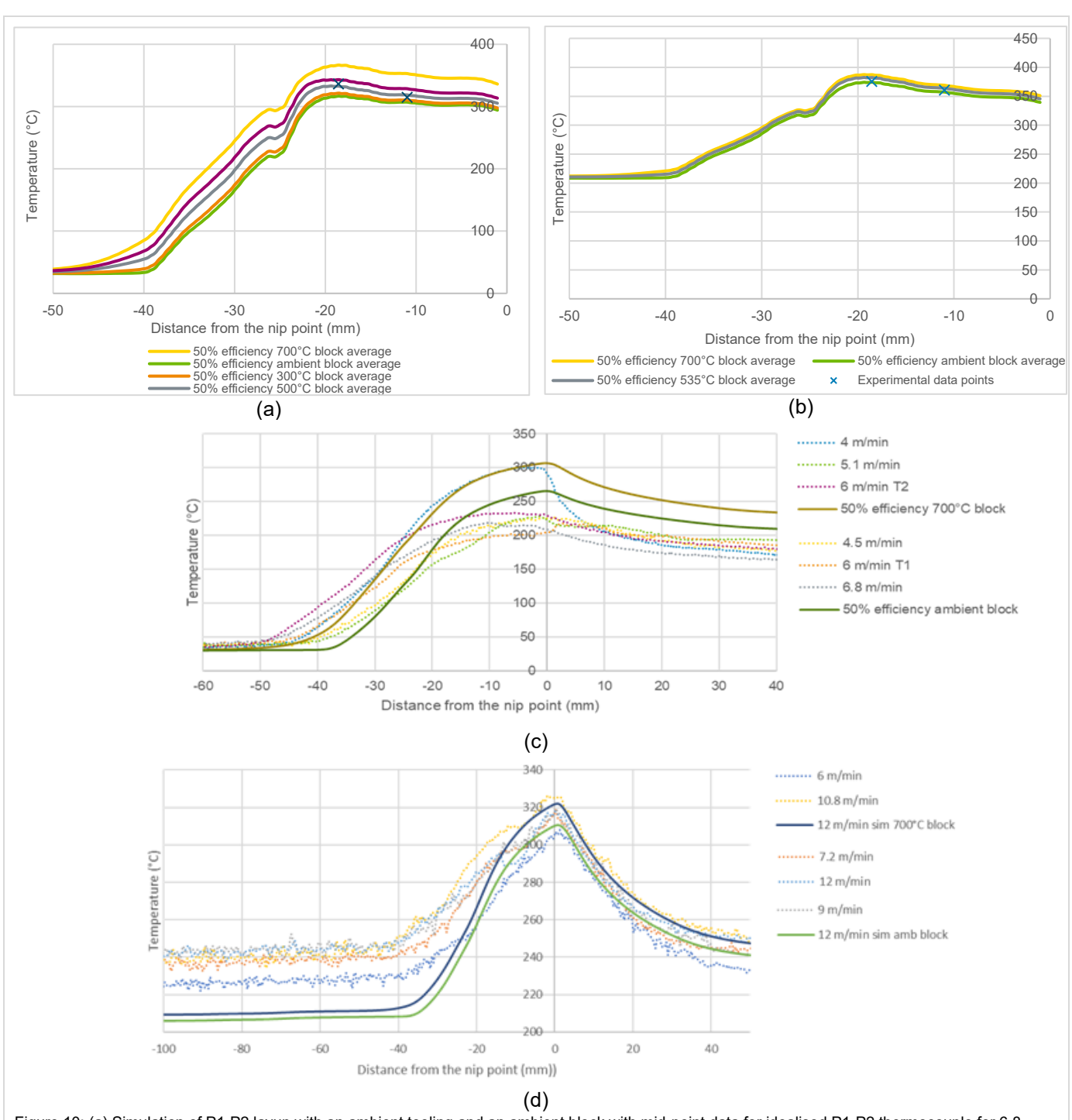
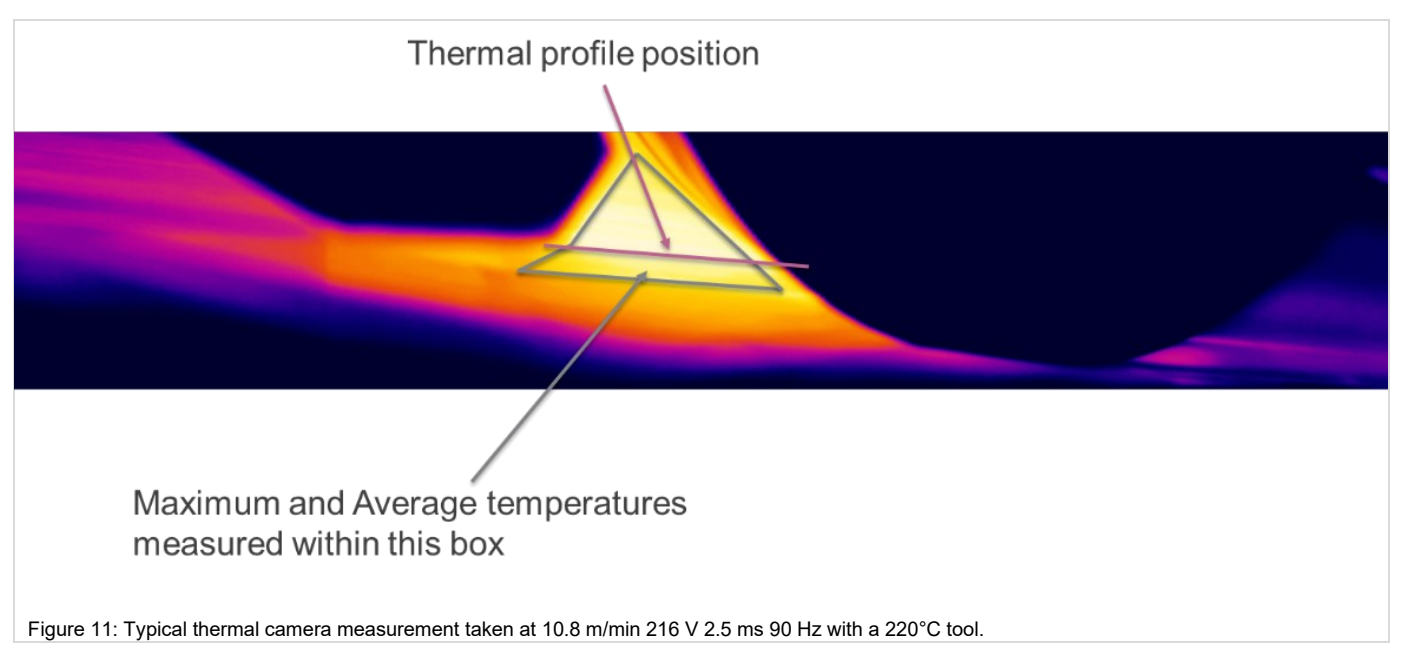


Figure 10: (a) Simulation of P1-P2 layup with an ambient tooling and an ambient block with mid-point data for idealised P1-P2 thermocouple for 6.8 m/min 219 V 90 Hz 2.5 ms pulse parameters. (b) Simulation of P1-P2 layup with 220°C tooling for and idealised P1-P2 thermocouple with mid-point data and pulse parameters of 12 m/min 219 V 90 Hz 2.5 ms. Comparison between experimental thermocouple measurements and simulation data for P1-P2 layup for the following: (c) S-P1 thermocouple ambient tooling, (d) S-P1 thermocouple 220°C tooling.





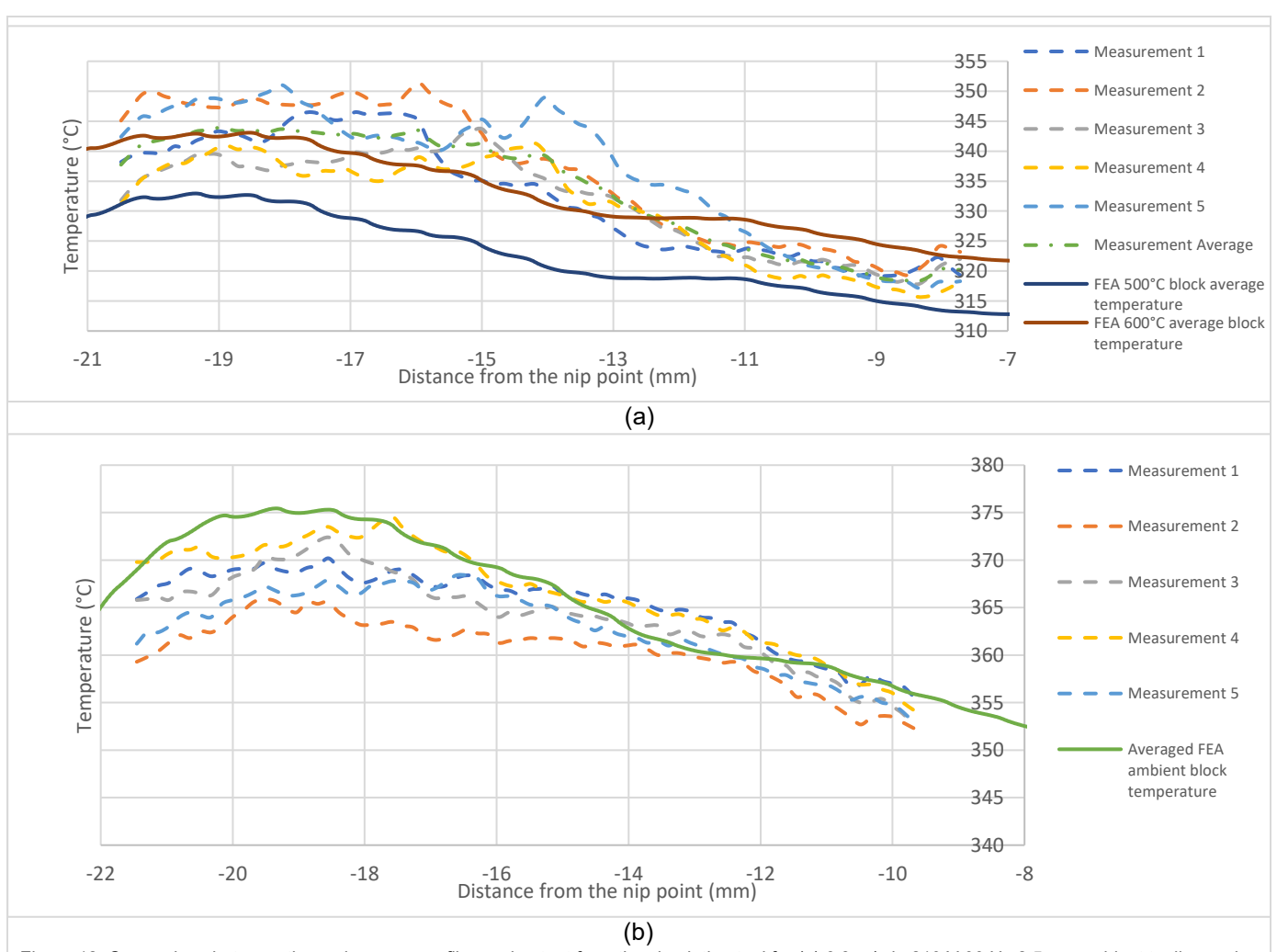


Figure 12: Comparison between thermal camera profiles and output from the simulation tool for (a) 6.8 m/min 219 V 90 Hz 2.5 ms ambient tooling and (b) 10.8 m/min 208 V 90 Hz 2.5 ms 220°C heated tooling.



Table 1. Optical Efficiency estimations of pulsed xenon flashlamp system between 140 V and 200 V.

Set Voltage (V)	Measured Wattage 250 to 1100 nm (W)	Corrected Wattage 250 to 1700 nm (W)	Optical Pulse Energy (J)	Exiting Pulse Energy (J)	Optical Efficiency of rays from the Flashlamp/Flow Tube Assembly to Exiting the Head
140	21.84	22.99	3.5	2.30	65.68%
160	36.97	38.92	5.6	3.89	69.50%
180	54.30	57.16	8.44	5.72	67.72%
200	78.75	82.90	12.08	8.29	68.62%
Predicted	68.02%				

Table 2: Thermal diffusivity parameters of constituent materials used in master AFP simulation.

Material	Specific Heat Capacity	Thermal Conductivity	Density (g/cm <sup>3</sup> )	
	(J/kg K)	(W/m K)		
Thermalimide	1130	0.29	1.47	
Silicone Roller	1070	0.245	1.12	
Fiberglass	893 at 20°C	0.06	1.1	
	1015 at 200°C			
Aluminium Tooling	880 at 22°C	125 at 22°C	2.66	
_	1100 at 480°C	167 at 500°C		

Table 3: Mean Temperature measurements and simulation tool predictions for different layup conditions at 90 Hz 2.5 ms with an ambient and 220°C heated tool.

Flash Conditions	Tool Temperature	Mean Maximum surface temperature (°C)	Predicted maximum temperature on substrate (°C)	Difference between simulation and thermal measurements (°C)	Predicted nip point temperature on substrate
		( 0)	substrate ( C)	measurements ( C)	(°C)
195 V 4 m/min	Ambient	333.9	336.20	3.30	327.25
198 V 4.5 m/min	Ambient	343.1	330.27	-12.83	313.34
200 V 5.1 m/min	Ambient	331.7	329.45	-2.25	303.38
219 V 6.8 m/min	Ambient	336.2	332.70	-3.50	311.83
186 V 6 m/min	220°C	375.8	380.44	4.64	364.37
193 V 7.2 m/min	220°C	373.8	378.32	4.52	357.60
204 V 9 m/min	220°C	376.5	380.36	3.86	353.97
209 V 10.8 m/min	220°C	376.9	375.32	-1.58	342.52